This article has been accepted for publication in a future issue of this journal, but has not been fully edited. Content may change prior to final publication. Citation information: DOI 10.1109/TPEL.2016.2598284, IEEE Transactions on Power Electronics

Fine Tuning of an Inductive Link Through a Voltage-Controlled Capacitance

R. W. Porto[1], *IEEE Student Member*, V. J. Brusamarello[1], *Member, IEEE*, L. A. Pereira[1], F. R. Sousa[2], *Member, IEEE*
Electrical Engineering Department - Federal University of Rio Grande do Sul,
Av. Osvaldo Aranha, 103, 90035-190, Porto Alegre, RS, Brazil[1]
Electrical Engineering Department - Federal University of Santa Catarina,
88040-900, Florianopolis, SC, Brazil[2]
Email: {rangel}@ieee.org, {wolff.porto, valner.brusamarello, lapereira}@ufrgs.br

***Abstract*—Wireless power transfer is a technique usually based on an inductive link, used for delivering energy to remote devices. The power of different applications ranges from microwatts to hundreds of kilowatts, e.g. in biomedical implants and electric vehicles. The transferred power is highly dependent on the relative position between the inductive link coils. Many studies have been presented considering static or quasi-static conditions, based on a fixed tuned circuit. However, when the coils are not stationary, the inductive link must be dynamically tuned to keep the designed output power. This paper presents a methodology for dynamically tune the inductive link by means of a variable capacitance. A voltage controlled capacitance using concepts of negative impedance converter and capacitance multiplier is proposed. The phase angle between the input voltage and current is used as the error signal to control the variable capacitance and keep the output power operating point. The experimental evaluation shows that the proposed methodology can significantly improve the power delivered to the load in comparison to a fixed inductive link.**

***Index Terms*—Inductive power transfer; electromagnetic coupling; optimization; voltage-controlled capacitance.**

I. Introduction

In recent years, a growing number of papers have been published on *wireless power transfer* (WPT), although the underlying physical principles are known since a long time. Beginning with the pioneering work of Nicola Tesla, the technology of WPT has evolved and its potential field of application nowadays includes many areas such as public transportation and biomedical devices. Although the energy transfer over long distances with high efficiency is not yet possible, many modern applications would benefit from power supplies without the presence of cables. WPT over short distances has been used in several applications requiring charging, such as: biomedical implants and devices [1]–[6], consumer electronics, pads for mobile devices [7], and electric vehicles [8]–[11].

One of the key-points for the development of WPT systems is the design of the coupling circuits. Although design procedures share similarities, each specific application imposes different design constraints, requiring a particular design procedure [12]. For instance, in biomedical applications the area available for the receiver coil is an important concern for the designer because it is very restricted [13], [14].

A typical WPT system contains a core inductive link connected to the power source and to the load through a matching impedance network. This network is usually composed of capacitors in order to tune the circuit. This is a fundamental characteristic of wireless transfer energy, where the capacitors should be chosen to maximize the power transfer or to maximize the efficiency of the inductive link. In [15], a numerical method for computing a network with four capacitors is proposed considering a static load connected to the output of the inductive link. However, usual applications have dynamic loads and the relative position between coils may change, which requires to vary the working frequency, or other circuit parameter, to keep the system tuned. That means, the inductive link must be tuned dynamically to ensure optimal performance under varying load. A number of different techniques of dynamic tuning may be found in literature, such as active tuning [16], frequency sweeping [17], saturable variable inductances [18], network of switching capacitors [19], among others [20], [21].

This article presents a dynamic and controllable capacitive network, which is implemented with a Voltage-Controlled Capacitor (VCCAP) based on capacitance multiplier and Negative Impedance Converter (NIC) concepts for tuning a wireless power system. The adapted network tracks the changes of the load caused by the variations of the magnetic coupling. The experimental variations of the magnetic coupling coefficient (k) were produced by changing the relative position between the transmitter and receiver coils ranging from $k = 0.2$ to $k = 0.8$ approximately. Initially, the analysis of the inductive link composed of a pair of coils is presented, as well as the analysis of the position of a variable capacitor in the matching capacitive network. Disregarding the non idealities of the input power source, as well the losses added by the active circuits, the inductive link can be tuned to deliver the maximum power to a variable load or a variable coupling coefficient. In addition, the paper presents the design of a voltage-controlled capacitance and a control strategy which can keep the inductive link tuned even under disturbances, detected as a phase shift between the input current and voltage.

This article has been accepted for publication in a future issue of this journal, but has not been fully edited. Content may change prior to final publication. Citation information: DOI 10.1109/TPEL.2016.2598284, IEEE Transactions on Power Electronics

Finally, experimental results are presented and compared with results obtained with a similar system using fixed capacitances. The main contributions of this paper are (1) the application of a capacitance multiplier and a Negative Impedance Converter (NIC) to dynamically tune an inductive link within a predefined range and (2) a novel methodology to continuously adapt the inductive link when the position of the coils changes.

II. Inductive Link Modeling and Design

A magnetically coupled system (composed of two coils) is usually represented by the following three inductances: L_1 (primary or transmitter coil), L_2 (secondary or receiver coil), and M (mutual inductance), which mainly depends on the relative position between the coils. The equivalent T-circuit of an inductive link shown in Fig. 1 is commonly used to model transformers. In order to maximize the Power Transferred to the Load (PDL) (or optionally the power transfer efficiency), a matching capacitive network (C_1 and C_2) is connected between the input power source (V_S) and the primary coil. Yet another matching capacitive network (C_3 and C_4) is connected between the secondary coil and the load (Z_L). The use of three or four capacitors can produce higher values of PDL than matching networks composed by one or two capacitors [15]. Compared to the case of one or two capacitors, using four capacitors, the circuit becomes more flexible and thus can be easily adjusted to the required output power. Therefore, we have chosen to use a network made up of four capacitors.

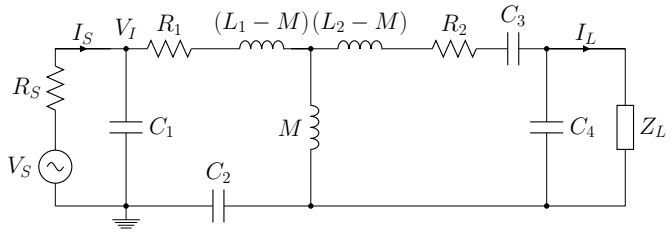

Fig. 1. Inductive link represented by the equivalent T-circuit and the matching network. V_S is the magnitude of the input voltage source with internal resistance R_S; L_1 and L_2 are the self-inductances of the primary and the secondary coil, respectively; R_1 and R_2 represent the joule losses of the coils.

The mutual inductance M is defined by:

$$M = k\sqrt{L_1 L_2} \tag{1}$$

where k is the magnetic coupling coefficient. By applying the Kirchhoff's Laws to the circuit in Fig. 1, the following expression results for the load current $\bar{I_L}$:

$$\bar{I_L} = \frac{j\omega M\left(\frac{V_S}{j\omega R_S C_1+1}\right)}{\left[F(j\omega)\cdot G(j\omega)+\left(\omega M\right)^2\right]\left(j\omega \bar{Z_L} C_4+1\right)} \tag{2}$$

where

$$F(j\omega) = R_2 + j\omega L_2 + \frac{1}{j\omega C_3} + \frac{\bar{Z_L}}{j\omega \bar{Z_L} C_4 + 1} \tag{3}$$

$$G(j\omega) = R_1 + j\omega L_1 + \frac{1}{j\omega C_2} + \frac{R_S}{j\omega R_S C_1 + 1} \tag{4}$$

Therefore, the power P_L at the load $\bar{Z_L}$ can be calculated by:

$$P_L = \frac{1}{2}\left|\bar{I_L}\right|^2 \cdot R_L \tag{5}$$

where R_L is the real part of $\bar{Z_L}$.

A. Inductive Link Design

The first step to design the inductive link is to define the dimensions of the secondary coil, which is constrained by the available space. In the case of Printed Circuit Board (PCB) coils, the manufacturing process imposes certain limits on the spacing between consecutive traces and on the width of each trace. Thus, the maximum number of turns of the secondary coil, N_2, is essentially determined by the mentioned geometrical constraints. According to the concepts described in [22], a receiver coil has been adopted with $38\,\mathrm{mm}$ external diameter, space between traces of $0.25\,\mathrm{mm}$ and trace width of $0.25\,\mathrm{mm}$. With these dimensions, the inductance of receiver coil with $N_2 = 38$ is $L_2 = 18.6\,\mu\mathrm{H}$, obtained through the Lyle's Method [23]. The parasitic resistance is estimated to $R_2 = 8.8\,\Omega$ for copper traces of 1 oz thickness.

The transmitter coil described in [22] has $45\,\mathrm{mm}$ of external diameter and 45 turns (N_1). The copper traces dimensions are the same of those described for the receiver coil. Thus, the inductance is $L_1 = 28.7\,\mu\mathrm{H}$ and its parasitic resistance $R_1 = 11\,\Omega$. When the transmitter and receiver coils are aligned and separated by $z = 3\,\mathrm{mm}$, the magnetic coupling factor k can be estimated by using the methods described in [23], or through the finite element method, resulting in $k = 0.65$ and $M = 15\,\mu\mathrm{H}$.

Once the distance between coils z (and consequently k), as well as the load Z_L (not necessarily a resistance), the input voltage source amplitude V_S (with its internal resistance R_S), and the working frequency f are all defined, optimization methods can be used to find the best capacitors for the matching network which maximize the objective function PDL. The algorithm presented in [15] finds capacitance values defined by the standardized E-24 series [24], which subdivides the interval from 1 to 10 into 24 steps. In this work, the search space of possible values of capacitance were limited by the IEC 60063 E24 series multiplied by 10^{-12} up to 10^{-4}, which gives a total of 216 possibilities to each capacitor (2176782336 to the 4 capacitors). Considering $V_S = 10\,\mathrm{V}$, $R_S = 1\,\Omega$, $R_L = 47\,\Omega$ and $f = 500\,\mathrm{kHz}$, the optimized capacitors are: $C_1 = 1\,\mathrm{pF}$, $C_2 = 4.7\,\mathrm{nF}$, $C_3 = 100\,\mathrm{nF}$, and $C_4 = 120\,\mathrm{pF}$.

B. Power Transferred to the Load

As the inductances of the primary and secondary coils are constant values, (5) can be maximized by varying the excitation frequency (f) or changing the matching network capacitors [19]. When the application imposes a fixed f and the available space constraint does not allow complex circuitry

This article has been accepted for publication in a future issue of this journal, but has not been fully edited. Content may change prior to final publication. Citation information: DOI 10.1109/TPEL.2016.2598284, IEEE Transactions on Power Electronics

at secondary side of the link, it is necessary to change the capacitive matching network at the primary side to reach the maximum PDL. As shown in Fig. 1 the capacitor C_1 is basically in parallel to the input source V_S , making it less effective in tuning the inductive link when R_S tends to zero. Thus, the capacitor C_2 can be used as a variable component on the primary side to tune the circuit in the event of a disturbance in the circuit, such as a load variation.

Considering the inductive link design described in II-A, the mesh equations of circuit shown in Fig. 1 can be calculated as a funcion of magnetic coupling coefficient k and the capacitor C_2. In Fig. 2 we can see the contour plots of P_L calculated using (5). One should notice that there is an optimum value of C_2 for each k. These points are highlighted in Fig. 2. On the other hand, we can plot P_L and the phase of the input current $\bar{I}_S$, both as a function of C_2 as shown in Fig. 3. One should notice that for a specific working frequency and k, there is an unique value for C_2 that maximizes P_L. At this point the reactive inductances of the link are cancelled by the capacitive network once the resonant point is reached. In Fig. 3 one should notice that when P_L reaches a maximum (for a specific k) the phase of the input current (θ_{Is}) related to the input voltage V_I is zero.

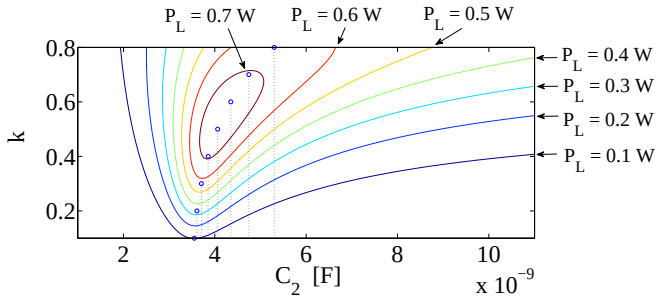

Fig. 2. Contour plot of power at the load (P_L) as function of magnetic coupling coefficient k and the capacitor C_2.

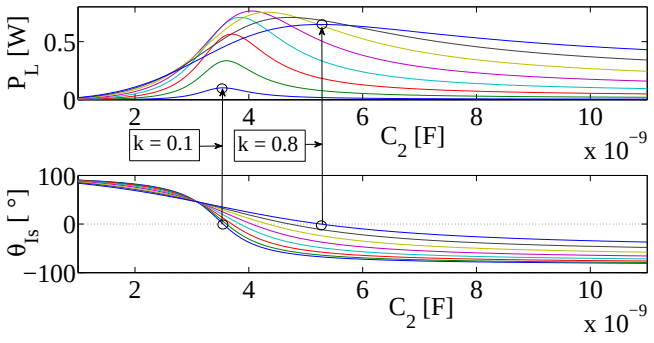

Fig. 3. Power at the load (P_L) and phase of input current (I_S) as a function of the capacitor C_2.

The optimum value of C_2 (C_{2opt}) can be obtained by taking the derivative of (5) with respect to C_2 and equaling it to zero. Thus, the expression for C_{2opt} that maximizes the output power P_L is:

$$C_{2opt} = \frac{\alpha^2 + \beta^2}{\omega[\gamma(\alpha^2 + \beta^2) - \beta(\omega M)^2]} \tag{6}$$

where α, β and γ are given as:

$$\alpha = R_2 + \frac{R_L}{1 + (\omega R_L C_4)^2} \tag{7}$$

$$\beta = \omega L_2 - \frac{1}{\omega C_3} - \frac{\omega Z_L^2 C_4}{1 + (\omega Z_L C_4)^2} \tag{8}$$

$$\gamma = \omega L_1 - \frac{\omega R_S^2 C_1}{1 + (\omega R_S C_1)^2} \tag{9}$$

Table I shows the optimum values C_{2opt} for some discrete values of k ranging from 0.15 to 0.85. The columns V_c and I_c show the voltage and current in the capacitor C_2, respectively. The design of the electronic devices used to vary or change the capacitance C_2 must consider the limits given by V_c and I_c. Furthermore, these devices must withstand $108.2\,\mathrm{V}_{pp}$ and $1.214\,\mathrm{A}_{pp}$ at the worst case of magnetic coupling coefficient ($k = 0.15$).

TABLE I
VALUES OF C_{2opt} AND ITS VOLTAGE (V_c) AND CURRENT (I_c) AS FUNCTION OF SOME DISCRETE VALUES OF k

k	$C_{2opt}[nF]$	$V_c[Vpp]$	$I_c[App]$
0.15	3.57	108.2	1.214
0.25	3.65	94.8	1.087
0.35	3.77	79.3	0.939
0.45	3.94	64.2	0.795
0.55	4.18	50.7	0.666
0.65	4.51	39.4	0.559
0.75	4.96	30.1	0.469
0.85	5.60	22.6	0.397

III. Dynamic Tuning Strategy

Although the power delivered to the load can be maximized by optimizing the matching capacitors of the link (considering fixed inductances of coils), they cannot be changed after the compensation for a specific operation point. Nonetheless, there are alternative ways to change the optimum point of operation. For instance, by changing the excitation frequency [17] or switching the capacitors of the compensation network [19], the circuit can be tuned again and a new operation point attained. The resonance of the primary side (minimum phase between voltage and current) minimizes the VA rating of the power supply and for most applications the maximum power transfer capability can be achieved by operating at the zero-phase-angle (ZPA) where not only the inductance of the primary side of the link is compensated but also the reflected impedance from the secondary side [25]. Thus, in order to detect that the circuit is operating at the maximal power transfer capability, the phase between the input voltage ($\bar{V}_I$) and input current ($\bar{I}_S$) can be monitored at the primary side of the link and used to modify the value of C_2 as shown in Fig. 4.

The automatic phase control of the inductive link can be implemented according to the block diagram depicted in Fig. 5. A phase comparison between $\bar{V}_I$ and $\bar{I}_S$ is necessary

This article has been accepted for publication in a future issue of this journal, but has not been fully edited. Content may change prior to final publication. Citation information: DOI 10.1109/TPEL.2016.2598284, IEEE Transactions on Power Electronics

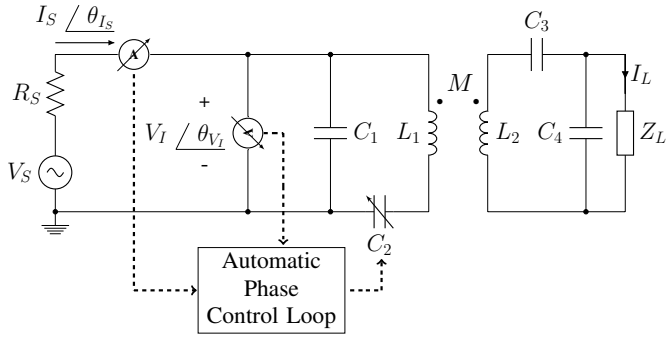

Fig. 4. Dynamic tuning strategy by means of a variable capacitance C_2 at primary side of the inductive link.

to detect the maximal power transfer capability. The phase difference ($\phi = \theta_{V_I} - \theta_{I_S}$) can be measured and converted to a continuous voltage by the scheme described in [26]. A Proportional-Integral (PI) controller is place afterwards the phase comparison in order to cancel the steady state error. The output signal of the PI controller is V_{ctrl}, which is used to control the Voltage-Controlled Capacitor (VCCAP) C_2. The changing value of C_2 can modify the phase θ_{I_S}, as shown in Fig. 3. This relationship is represented by $T(s)$, which is considered a transfer function from the inductive link.

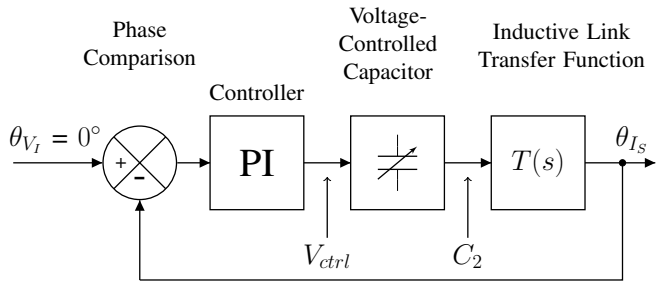

Fig. 5. Automatic phase control loop.

A. Voltage-Controlled Capacitor (VCCAP) Circuit Design

A convenient way to implement the variable capacitance C_2 is by using a control voltage. Thus, a VCCAP can be implemented through a Negative Impedance Converter (NIC) or a capacitance multiplier circuit. The general concept is depicted in Fig. 6. The following analysis considers a voltage-controlled amplifier (VGA) whose first-order transfer function, $\bar{A} = f(V_{ctrl})$ is given by:

$$\bar{A} = \frac{A_o}{1 + j\omega\tau} \tag{10}$$

where A_o is the DC-voltage gain and $1/\tau$ is the dominant pole of the VGA.

If the input impedance and output impedance of the VGA are neglected, the input impedance $\bar{Z_{in}}$ of the proposed circuit is calculated as follows:

$$\bar{Z_{in}} = \frac{1}{j\omega \cdot C_o} \cdot \frac{1 + j\omega\tau}{(1 - A_o) + j\omega\tau} \tag{11}$$

where C_o is a reference capacitor.

In order to disregard the influence of the frequency on the value of the variable capacitor, the pole ($1/\tau$) of $\bar{A}$ has to be located at least one decade above the working frequency. If this requirement is met, $\bar{Z_{in}}$ will be simplified as:

$$\bar{Z_{in}} = \frac{1}{j\omega \cdot C_o \cdot (1 - A_o)} \tag{12}$$

where A_o is the DC-gain of the amplifier controlled by the voltage V_{ctrl}.

Thus, the equivalent capacitance calculated from the input terminals is given by:

$$C_{adj} = C_o \cdot (1 - A_o) \tag{13}$$

When the values of A_o are lower than unity, the circuit of Fig. 6 works as a capacitance multiplier. On the other hand, when the values of A_o are higher than unity, the proposed circuit works as a NIC.

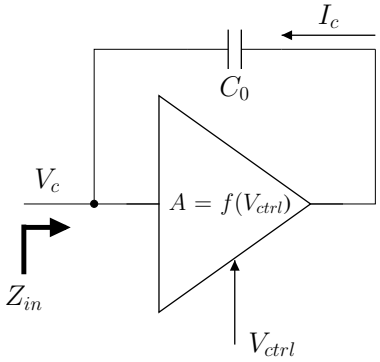

Fig. 6. Voltage-controlled negative impedance converter topology.

In case of $A_o = 1$ the input impedance $\bar{Z_{in}}$ tends to infinity and the capacitance C_{adj} approximates to zero, which is useless for the inductive link. To overcome this problem, the circuit of Fig. 6 can be connected in parallel to a fixed capacitor C_{2F}. Thus, the total equivalent capacitance is calculated by:

$$C_2 = C_{2F} + C_{adj} \tag{14}$$

where C_{adj} can be either positive or negative according to (13).

The VCCAP can be implemented according to the block diagram shown in Fig. 7. There are several methods to implement a VGA. One of those methods consists of using a four-quadrant multiplier. The analog multiplier MPY634 was chosen for this purpose. A voltage divider (R_A and R_B) is necessary at the input of the multiplier in order to keep the voltage amplitude within the allowed range. In addition, a phase correction stage is introduced in the block diagram to cancel the phase difference between the signals V_c and V_o shown in Fig. 7. One should notice that the VGA DC-gain A_o has to be a real number, according (13). Finally, an output stage has to be included in the circuit in order to reduce the output impedance of the VGA and improve the output current

This article has been accepted for publication in a future issue of this journal, but has not been fully edited. Content may change prior to final publication. Citation information: DOI 10.1109/TPEL.2016.2598284, IEEE Transactions on Power Electronics

capability. Thus, the proposed VCCAP circuit has the ideal frequency-independent gain $A_o = \frac{V_o}{V_c}$ according to:

$$A_o = \frac{R_A}{R_A + R_B} \cdot G_o \cdot V_{ctrl} \tag{15}$$

where G_o is the combined gain of the multiplier, phase correction and output stages.

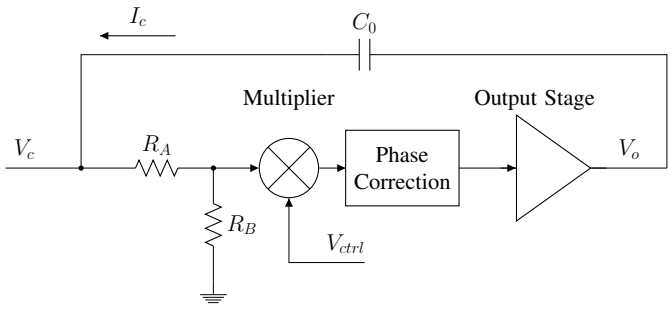

Fig. 7. VCCAP block diagram.

The design of the proposed VCCAP can be summarized according to the flowchart of Fig. 8. The geometrical specifications and their constraints impacts on the size of the coils. In addition, the electrical specifications such as the output power and the load complete the specifications for the design of the inductive link. The compensation capacitors are obtained for a specific k in order to maximize the output power. Then, it should be considered that some parameters of the link may vary, such as the load Z_L or the magnetic coupling coefficient k. Here, we have considered a variation in k, which impacts on the output power. The range of optimum values for C_2 (C_{2opt}) can be obtained by (6).

In the presented case of study we consider the inductive link for powering the wireless sensor node described in [22], where the typical distance between coils is $z = 3\,\mathrm{mm}$. In this case, when the coils are aligned, the magnetic coupling coefficient is $k = 0.65$. The VCCAP can remain inactive around this operating point. Therefore, it becomes possible to set the VGA gain as $A_o = 1$ in (13) for $C_{adj} = 0$ and hence $C_{2F} = C_2 = 4.7\,\mathrm{nF}$ (for the case study presented is this work). Once the value of C_o is assigned, the range of VGA gain A_o is calculated by (13). Finally, the range of the control voltage V_{crtl} necessary to maximize the output power is calculated by (15).

The complete implementation of the VCCAP suitable for the inductive link described in section II-A is shown in Fig. 9. The output stage must be implemented with a high voltage and high speed power operational amplifier (in this work TI 3584). The phase correction stage is implemented by a second-order all-pass filter with unity-gain, phase lead and central frequency of $500\,\mathrm{kHz}$.

B. Phase Detection Scheme and phase control loop

The phase detection scheme shown in Fig. 10 is based on the integrated circuit AD8302, which is used for radio frequency gain and phase detection [26]. The phase difference (ϕ) between the signals V_A (sample of V_I) and V_B (sample of I_S) is detected and an output DC-voltage V_{phs} is produced at the rate 10 mV/°. The input current I_S is measured by using a shunt resistor R_{sh} and a differential amplifier. The current measurement signal is attenuated by the voltage divider R_7 and R_8, which is necessary to keep the input voltage amplitude of the AD8302 within the allowed range. The input voltage of the inductive link V_I is buffered and afterwards attenuated by the voltage divider R_9 and R_{10}.

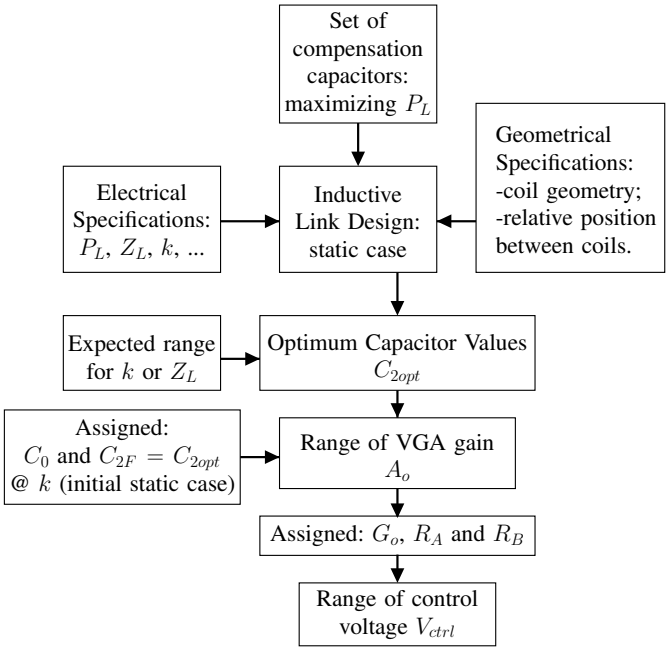

Fig. 8. Flowchart that summarizes the VCCAP design.

The signal V_{phs} expresses an estimate of the phase difference (in degrees) between the input voltage V_I and input current I_S according to the following equation [26]:

$$V_{phs} = 1.8 - 10 \cdot 10^{-3} \cdot |\phi| \tag{16}$$

where $\phi \approx \theta_{V_I} - \theta_{I_S}$.

The phase comparison of Fig. 5 can be implemented by a differential amplifier as shown in Fig. 11. The reference voltage V_{set} is used as a setpoint and the signal error from the output of the differential amplifier is integrated in the next stage, establishing a PI controller. The zener diode D1 limits the control voltage V_{ctrl} up to $8.2\,\mathrm{V}$.

IV. Experimental Evaluation and Results

A. Evaluation of the VCCAP

The VCCAP has been experimentally evaluated by measuring firstly the input impedance of the circuit according to Fig. 12. A sinusoidal wave (V_g) of $10\,\mathrm{V}_{pp}$ and $500\,\mathrm{kHz}$ has been applied at the input of the circuit. A series resistor (R_{sh}) of $15\,\Omega$ has been placed in order to access the input current I_{in}. The absolute value of input impedance has been calculated by $\left|Z_{in}\right| = \frac{V_2}{V_1}$, where V_1 and V_2 have been measured with a Tektronix DPO7104 oscilloscope. Thus, the input equivalent resistance and input equivalent capacitance are given by respectively:

This article has been accepted for publication in a future issue of this journal, but has not been fully edited. Content may change prior to final publication. Citation information: DOI 10.1109/TPEL.2016.2598284, IEEE Transactions on Power Electronics

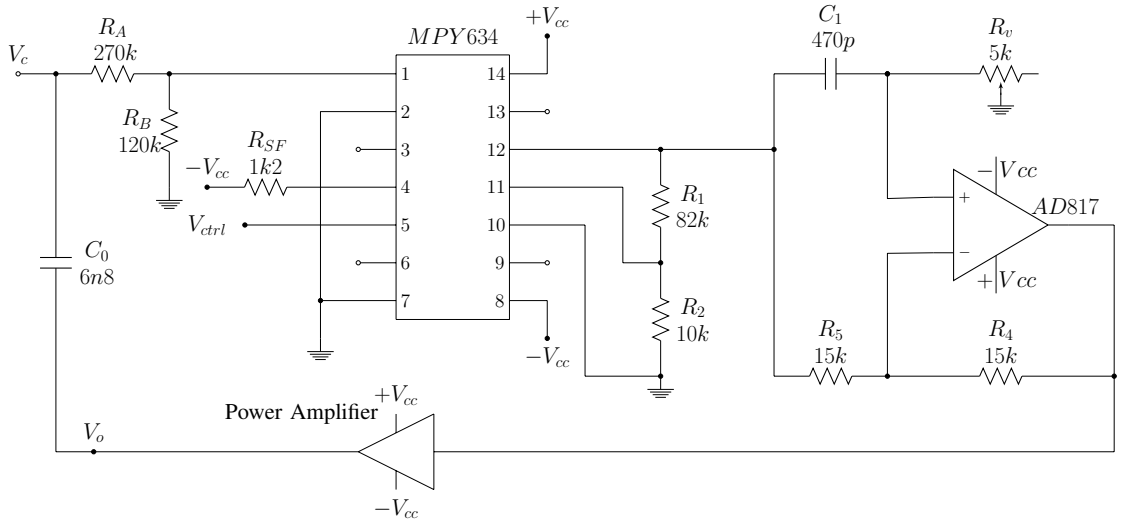

Fig. 9. VCCAP circuit.

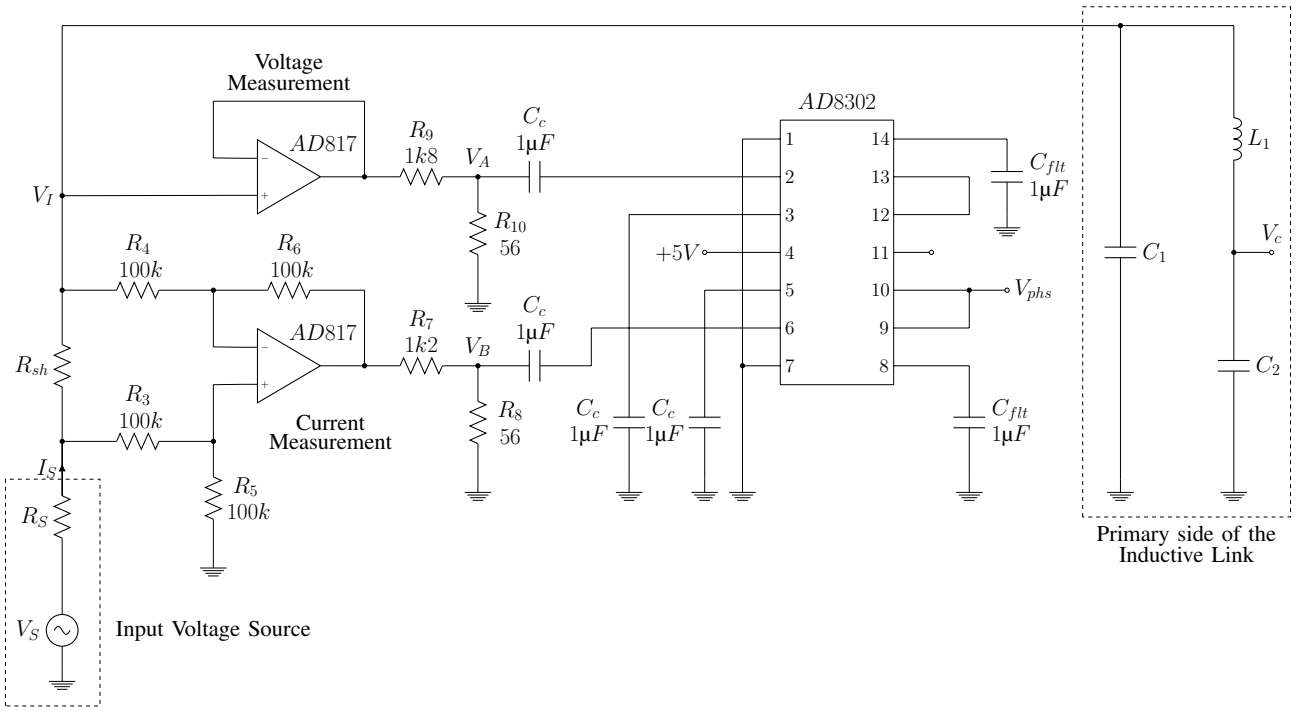

Fig. 10. Phase detection circuit.

$$R_{in} = \left|Z_{in}\right| \cdot \cos(\theta) \tag{17}$$

$$C_{adj} = \left[2 \cdot \pi \cdot f \cdot (\left|Z_{in}\right| \cdot \sin(\theta))\right]^{-1} \tag{18}$$

where θ is the phase difference between V_{in} and I_{in} which has been measured with the oscilloscope. Fig. 13 shows the results of (18) as a function of V_{ctrl} for a reference capacitor C_0 of $6.8\,\mathrm{nF}$. The difference in the slope of these curves can be attributed to nonlinearities in the blocks shown in Fig. 7.

The resistor R_c represents the Equivalent Series Resistance (ESR) of the reference capacitor C_0 and the output resistance of the VGA. Its effect is also reflected to the input terminals of the voltage-controlled capacitor, as shown in Fig. 14, where the calculations of (17) have been made as a function of V_{ctrl}. The circuit has shown to be unstable to V_{ctrl} greater than $4.7\,\mathrm{V}$.

B. Evaluation of the Magnetic Coupling Coefficient for Evenly Spaced and Misaligned Coils

An experimental setup has been developed for studying the effects of the distance between coils on the magnetic coupling coefficient k, which plays an important role for inductive link tuning. A Printed Circuit Board (PCB) Drill Machine has been used to control the position of the secondary coil. The

This article has been accepted for publication in a future issue of this journal, but has not been fully edited. Content may change prior to final publication. Citation information: DOI 10.1109/TPEL.2016.2598284, IEEE Transactions on Power Electronics

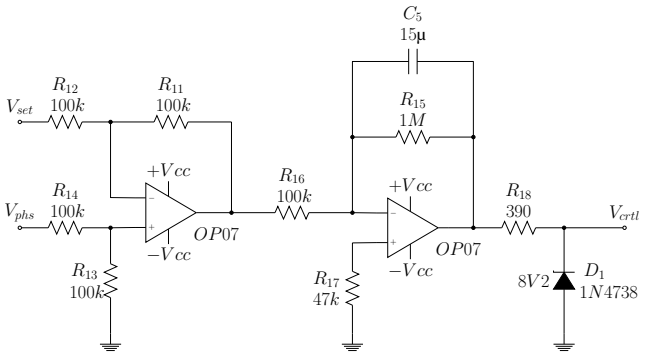

Fig. 11. Phase comparison and the PI controller.

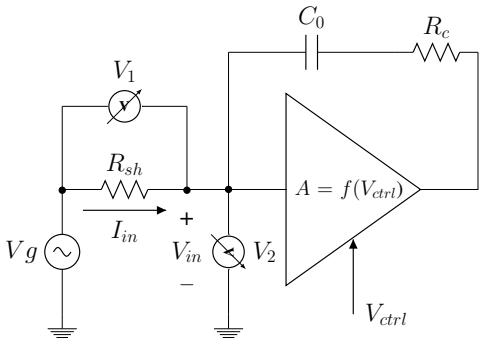

Fig. 12. Input impedance evaluation of the Voltage-Controlled Capacitor.

prototype is shown in Fig. 15. The coils were positioned far from the metal structures of the Drill Machine in order to avoid interference in the measurements.

The first experiment was carried out by varying the distance between coils d from $1\,\mathrm{mm}$ to $10\,\mathrm{mm}$ steps of $1\,\mathrm{mm}$ on parallel planes and aligned axes. Fig. 16 shows the approximate range of the magnetic coupling coefficient k from 0.3 to 0.8, which was estimated by using a sinusoidal wave (V_a) with amplitude of $10\,\mathrm{V}_{pp}$ and $500\,\mathrm{kHz}$ on the primary coil (without any capacitive compensation). For each relative position between coils the induced voltage on secondary coil (V_b) was measured without any capacitive compensation. Thus, the magnetic coupling coefficient was estimated (neglecting the parasitic resistances of the coils) by:

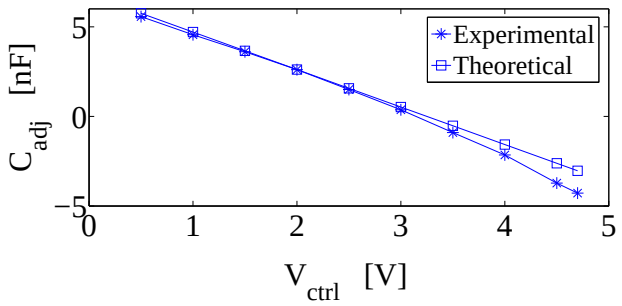

Fig. 13. Comparative results of the voltage controlled capacitor. Input equivalent capacitance C_{adj} as a function of the control voltage V_{ctrl}.

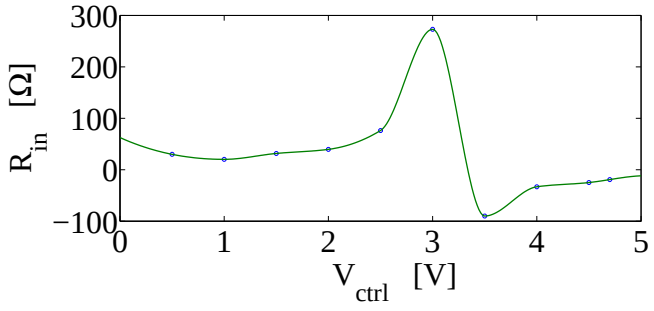

Fig. 14. Input equivalent resistance R_{in} as a function of the control voltage V_{ctrl}.

$$k = \frac{V_b}{V_a} \cdot \sqrt{\frac{L_1}{L_2}} \tag{19}$$

where V_a and V_b are the voltage amplitude of the primary and secondary coils, L_1 and L_2 are the inductances of primary and secondary coils, respectively.

The second experiment was conducted by setting a clearance of $3\,\mathrm{mm}$ between coils and moving the secondary coil along the horizontal plane of the PCB Drill Machine. The magnetic coupling coefficient k was estimated by (19) as a function of the position on the horizontal plane. As illustrated in Fig. 17, k decreases towards to zero while increasing the misalignment between the coils. These two experiments are valuable to evaluate the range of k which is one of the key factors for the design of the voltage-controlled capacitor.

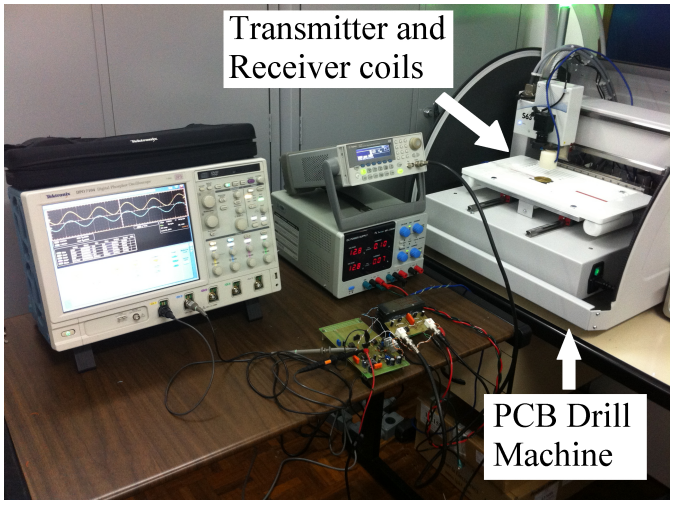

Fig. 15. Experimental Setup for the evaluation of k and the inductive link characterization.

C. Evaluation of the Dynamically Tuned Inductive Link

A sinusoidal input voltage (V_S) with amplitude of $20\,\mathrm{V}_{pp}$ and frequency $500\,\mathrm{kHz}$ has been applied to the proposed inductive link during the simulation. Fig. 18 shows the comparative results for load voltage V_L with the capacitor C_2 fixed and also dynamically adjusted. When C_2 is fixed at

This article has been accepted for publication in a future issue of this journal, but has not been fully edited. Content may change prior to final publication. Citation information: DOI 10.1109/TPEL.2016.2598284, IEEE Transactions on Power Electronics

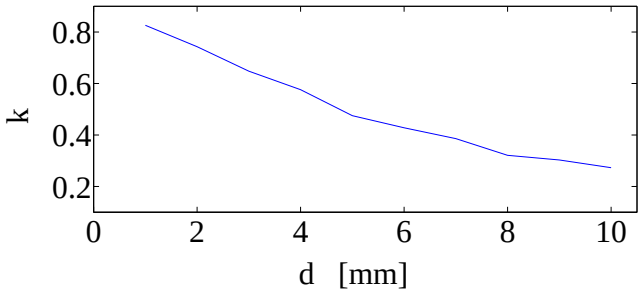

Fig. 16. Experimental results for k as a function of the distance d when the coils are parallel and aligned.

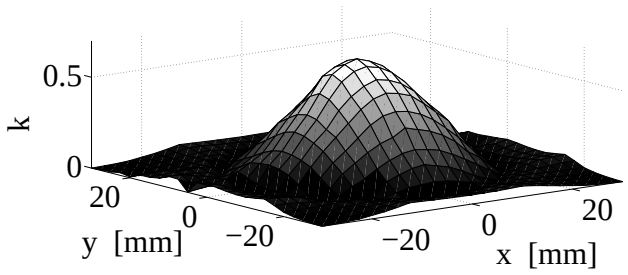

Fig. 17. Experimental results for k when the coils are separated by $3\,\mathrm{mm}$ and the receiver coil moves on the plane xy.

$4.7\,\mathrm{nF}$, we notice that V_L reaches a maximum at $k = 0.65$, as predicted in section II. As k decays the load voltage V_L decreases until $8.74\,\mathrm{V}_{pp}$, as indicated on Fig. 18. By using the proposed voltage-controlled capacitor, C_2 is properly adjusted, maximizing V_L for each k. Thus, for the lowest k studied in this work ($k = 0.273$) V_L rises from $8.74\,\mathrm{V}$ (without dynamic compensation) to $12.42\,\mathrm{V}$. Fig. 18 also highlights that the proposed method for inductive link tuning is mainly effective for $k < 0.65$.

The experimental evaluation has been conducted with a linear power amplifier that generates a sine wave as input voltage source (V_I) with $20\,\mathrm{V}_{pp}$ and $500\,\mathrm{kHz}$. The coils have been positioned in order to produce the values of k according to Fig. 16. The voltage measurements were taken at the secondary side of the link in a $47\,\Omega$ resistive load. The experimental results are also shown in Fig. 18. In case of fixed C_2, the experimental and simulated curves are similar. However, the simulated values of V_L are greater than in the experiment mainly because the ESR of the matching capacitors have been neglected in the simulation.

For the case of adjusted C_2, an improvement in V_L was observed, as predicted by the simulation. This is specially true for the lowest k studied in this work, where V_L rises up from $6.44\,\mathrm{V}$ to $10.80\,\mathrm{V}$, as shown in Fig. 18. As predicted by the simulation, the application of a variable capacitance at the primary side of the inductive link is effective for $k < 0.65$. At $k = 0.65$ the values of V_L should be approximately the same as shown in the simulation curves. However, in the experimental results at $k = 0.65$ one should notice a difference around $2\,\mathrm{V}$ between the adjusted C_2 and fixed C_2 curves. Some nonidealities were not taken into account in the simulation results, such as: the ESR of the fixed capacitors, nonlinearity of the curve $C_{adj} = f(V_{ctrl})$ (see Fig. 13), and the effect of the resistive part of the input impedance of VCCAP (see Fig. 14) on the primary side of the inductive link.

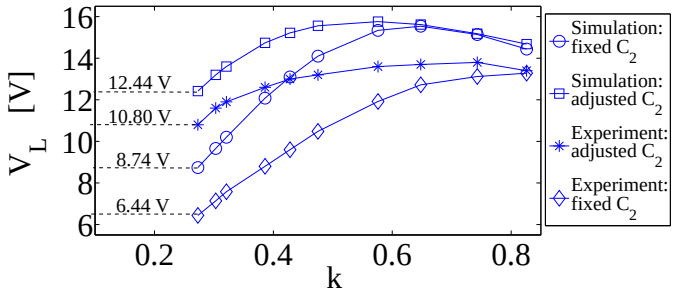

Fig. 18. Simulated and experimental results of load voltage V_L for fixed and adjusted C_2.

Fig. 19 shows the comparative results of ϕ. One should notice that the inductive link has been firstly designed to work at $k = 0.65$ and the capacitive compensation network has been chosen in order to maximize the output power (or V_L for fixed resistive load). Therefore, the phase ϕ should be close to zero. Even in the simulation results for fixed C_2, ϕ is close to $5°$. This error appears because the optimal solution for the output power requires capacitors values not available in the IEC 60063 standard [24]. When the capacitive compensation network is fixed, specially C_2, the inductive link is seen as a resistance at the input terminals at a specific k. In Fig. 19, for k greater than 0.7 the inductive link behaves like a capacitive load. Otherwise, for k less than 0.7 a inductive behaviour is seen at the primary side of the link. Fig. 19 also shows ϕ when C_2 is dynamically adjusted. In the range of k studied in this work the phase ϕ remains less than $2°$.

The experimental results of ϕ as a function of k for fixed and adjusted $C2$ are also shown in Fig. 19, which were quite close to the simulated curves. When the proposed VCCAP has been connected to the inductive link, the phase ϕ has remained stable and the error less than $5°$.

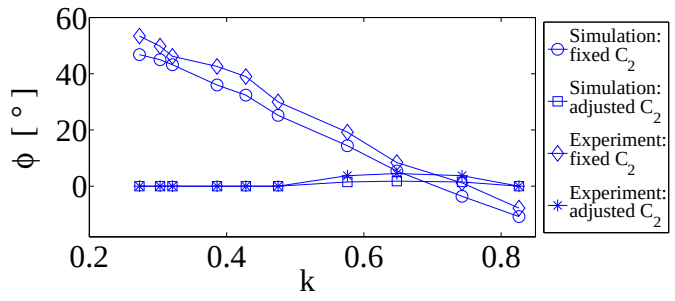

Fig. 19. Simulated and experimental results of ϕ for fixed and adjusted C_2.

The phase control loop has been evaluated by adjusting V_{set} (see Fig. 11) intentionally to $1.5\,\mathrm{V}$, which leads $\phi = 45°$. This setpoint has been arbitrarily chosen in order to show that the control loop will follow the reference. The distance

This article has been accepted for publication in a future issue of this journal, but has not been fully edited. Content may change prior to final publication. Citation information: DOI 10.1109/TPEL.2016.2598284, IEEE Transactions on Power Electronics

between coils has been varied from 3 mm to 9 mm. As they were aligned, the magnetic coupling coefficient has changed from $k = 0.3$ to $k = 0.6$, approximately (see Fig. 16). As the distance between coils increases, V_{ctrl} rises up to compensate the phase change (ϕ). Fig. 20 shows the effect of V_{ctrl} on the phase ϕ, which is represented by V_{phs} when the stimulus was introduced by the moving axis of the Drill Machine. One should notice that V_{phs} tends to stabilize at 1.5 V after a new distance between coils is reached. The transient response of V_{phs} shows an overshoot of 8% approximately.

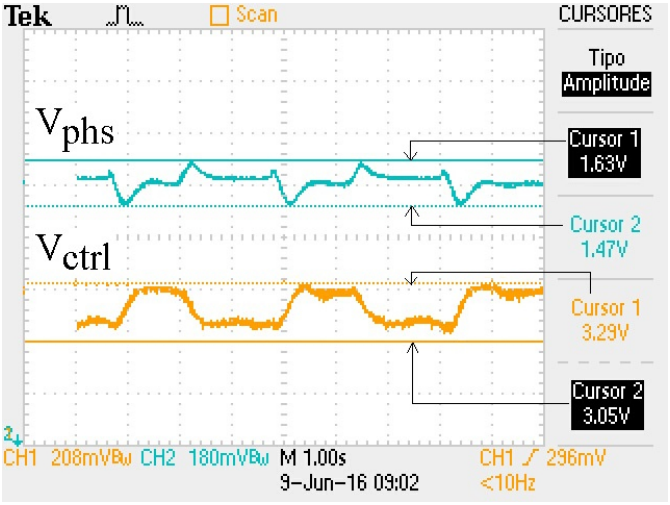

Fig. 20. Adapted image from the Tektronix TDS1001C oscilloscope screen. Waveforms of V_{ctrl} and V_{phs} when k varies from 0.3 to 0.6.

V. Conclusion

This paper has presented a methodology for tracking the maximum power transfer capability of an inductive link by using a VCCAP on the primary coil. This operation point is reached when the phase between the input voltage and input current is zero. As a case study, an inductive link has been design, simulated and implemented with the proposed circuit for varying the capacitance.

The coils of the prototype have been positioned in paralleled planes with their axes aligned. The distance between coils has been varied from 1 mm to 10 mm and the magnetic coupling coefficient k was estimated, emulating cases such as the misalignment of the coils. The range of k plays an important role for the design of the VCCAP because it determines the range of the capacitor (C_{2opt}). Once determined the range of C_{2opt} the blocks of the VCCAP can be designed. The insertion of a phase correction stage will depend on the phase lag of the multiplier and the used power amplifier. The obtained results presented in this paper, such as (6) are valid for the equivalent circuit of Fig. 1. For other configurations, the equations for I_L and C_{2opt} have to be adapted.

The inductive link has been designed and optimized for operating at a certain nominal distance between coils. In the experimental results, when the distance between coils is altered, and so the coupling coefficient, the VCCAP has shown to be effective for operating distances above the nominal ($k < 0.65$). Specifically at 10 mm ($k = 0.273$), the experimental results have shown an improvement of 67.7% in the output voltage V_L compared with a fixed capacitor network and the same inductive link.

Although the phase detection circuit has some limitations on detecting the maximum output power capability when the proposed circuit operates at closed loop, the results have shown that the system follows the reference and so, the inductive link is compensated. Future research will be conducted to improve the theoretical model of the VCCAP and the phase control system. The applicability of the proposed VCCAP for higher output power levels will be also a future concern.

Acknowledgment

We would like to thanks CAPES and FAPERGS - Fundação de Amparo a Pesquisa do Rio Grande do Sul, for the research support - PqG $2110 - 2551/13 - 0$.

References

[1] R. Wu, W. Li, H. Luo, J. K. O. Sin, and C. P. Yue, "Design and characterization of wireless power links for brain - machine interface applications," *IEEE Trans. Power Electron.*, vol. 29, no. 10, pp. 5462–5471, Jan. 2014.

[2] U. M. Jow and M. Ghovanloo, "Design and optimization of printed spiral coils for efficient transcutaneous inductive power transmission," *IEEE Trans. Biomed. Circuits Syst.*, vol. 1, no. 3, pp. 193–202, Sep. 2007.

[3] P. Li and R. Bashirullah, "A wireless power interface for rechargeable battery operated medical implants," *IEEE Trans. Circuits Syst. II, Exp. Briefs*, vol. 54, no. 10, pp. 912–916, Oct. 2007.

[4] T. Sun, X. Xie, G. Li, Y. Gu, Y. Deng, and Z. Wang, "A two-hop wireless power transfer system with an efficiency-enhanced power receiver for motion-free capsule endoscopy inspection," *IEEE Trans. Biomed. Eng*, vol. 59, no. 11, pp. 3247 – 3254, Nov. 2012.

[5] M. Kiani and M. Ghovanloo, "An rfid - based closed-loop wireless power transmission system for biomedical applications," *IEEE Trans. Circuits Syst. II, Exp. Briefs*, vol. 57, no. 4, pp. 260 – 264, Apr. 2010.

[6] P. Si, A. P. Hu, and S. Malpas, "A frequency control method for regulating wireless power to implantable devices," *IEEE Trans. Biomed. Circuits Syst.*, vol. 2, no. 1, pp. 22–29, Mar. 2008.

[7] E. Waffenschmidt and T. Staring, "Limitation of inductive power transfer for consumer applications," in *Proc. 13th European Conference on Power Electronics and Applications, 2009. EPE '09*. Barcelona: EPE, Sept 2009, pp. 1–10.

[8] S. Y. R. Hui, W. Zhong, and C. K. Lee, "A critical review of recent progress in mid-range wireless power transfer," *IEEE Trans. Power Electron.*, vol. 29, no. 9, pp. 4500–4511, Sept. 2014.

[9] J. Huh, S. W. Lee, W. Y. Lee, G. H. Cho, and C. T. Rim, "Narrow-width inductive power transfer system for online electrical vehicles," *IEEE Trans. Power Electron.*, vol. 26, no. 12, pp. 3666–3679, Dec. 2011.

[10] M. Budhia, G. A. Covic, and J. T. Boys, "Design and optimization of circular magnetic structures for lumped inductive power transfer systems," *IEEE Trans. Power Electron.*, vol. 26, no. 11, pp. 3096–3108, Nov. 2011.

[11] S. Ahn, J. Pak, T. Song, H. Lee, J. Byun, D. Kang, C. Choi, E. Kim, J. Ryu, M. Kim, Y. Cha, Y. Chun, C. Rim, J. Yim, D. Cho, and J. Kim, "Low frequency electromagnetic field reduction techniques for the on-line electric vehicle (olev)," in *IEEE International Symposium on Electromagnetic Compatibility*. IEEE, Jul. 2010, pp. 625 – 630.

[12] J. Masuch and M. D. Restituto, "Design constraints for the inductive power and data link of an implanted body sensor," in *European Conference on Circuit Theory and Design, 2009. ECCTD 2009.* IEEE, Aug. 2009, pp. 425–428.

[13] F. L. C. Riano and F. R. de Sousa, "Optimal design of energy efficient inductive links for powering implanted devices." in *2014 IEEE Topical Conference on Biomedical Wireless Technologies, Networks, and Sensing Systems (BioWireleSS),*. Newport Beach, CA.: IEEE, Jan. 2014, pp. 37–39.

[14] F. L. Cabrera and F. de Sousa, "Contactless characterization of a cmos integrated lc resonator for wireless power transferring," *IEEE Microw. Wireless Compon. Lett.*, vol. 25, no. 7, pp. 475–477, Jul. 2015.

[15] R. de Azambuja, V. J. Brusamarello, S. Haffner, and R. W. Porto, "Analysis and optimization of an inductive power transfer with a randomized method," *IEEE Trans. Instrum. Meas*, vol. 63, no. 5, pp. 1145 – 1152, May. 2014.

[16] Z. Pantic and S. M. Lukic, "Framework and topology for active tuning of parallel compensated receivers in power transfer systems," *IEEE Trans. Power Electron.*, vol. 27, no. 11, pp. 4503–4513, Nov. 2012.

[17] V. Brusamarello, Y. B. Blauth, R. de Azambuja, I. Muller, and F. R. de Sousa, "Power transfer with an inductive link and wireless tuning," *IEEE Trans. Instrum. Meas.*, vol. 62, no. 5, pp. 924 – 931, May. 2013.

[18] S. Aldhaher, P. Luk, and J. F. Whidborne, "Tuning class e inverters applied in inductive links using saturable reactors," *IEEE Trans. Power Electron.*, vol. 29, no. 6, pp. 2969–2978, Jun. 2014.

[19] Y. Lim, H. Tang, S. Lim, and J. Park, "An adaptive impedance-matching network based on a novel capacitor matrix for wireless power transfer," *IEEE Trans. Power Electron.*, vol. 29, no. 8, pp. 4403–4413, Aug. 2014.

[20] S. Aldhaher, P. Luk, and J. F. Whidborne, "Electronic tuning of misaligned coils in wireless power transfer systems," *IEEE Trans. Power Electron.*, vol. 29, no. 11, pp. 5975–5982, Nov. 2014.

[21] B. L. Cannon, J. F. Hoburg, D. D. Stancil, and S. C. Goldstein, "Magnetic resonant coupling as a potential means for wireless power transfer to multiple small receivers," *IEEE Trans. Power Electron.*, vol. 24, no. 7, pp. 1819–1825, Jul. 2009.

[22] R. W. Porto, V. J. Brusamarello, I. Muller, and F. R. Sousa, "Design and characterization of a power transfer inductive link for wireless sensor network nodes." in *IEEE International Instrumentation and Measurement Technology Conference (I2MTC)*, May 2015, pp. 1261–1266.

[23] F. W. Grover, *Inductance Calculations: working formulas and tables*. Dover Publications, Inc., 1946.

[24] *Preferred Number Series for Resistors and Capacitors*, IEC60063, IEC Std., 1963.

[25] C. Wang, O. H. Stielau, and G. A. Covic, "Design considerations for a contactless electric vehicle battery charger," *IEEE Trans. Ind. Electron.*, vol. 52, no. 5, pp. 1308 – 1314, Oct. 2005.

[26] Y. F. Yee and C. K. Chakrabarty, "Phase detection using ad8302 evaluation board in the superheterodyne microwave interferometer for line average plasma electron density measurements," *Measurement*, vol. 40, no. 9-10, pp. 849–853, Dec. 2007.